THE JOURNAL OF COMPARATIVE NEUROLOGY 504:583–598 (2007)

Projections of the Lateral Reticular Nucleus to the Cochlear Nucleus in Rats

XIPING ZHAN[1] AND DAVID K. RYUGO[1,2]*
[1]Department of Otolaryngology—Head and Neck Surgery, Center for Hearing and Balance, Johns Hopkins University School of Medicine, Baltimore, Maryland 21205
[2]Department of Neuroscience, Center for Hearing and Balance, Johns Hopkins University School of Medicine, Baltimore, Maryland 21205

ABSTRACT

The lateral reticular nucleus (LRN) resides in the rostral medulla and caudal pons, is implicated in cardiovascular regulation and cranial nerve reflexes, and gives rise to mossy fibers in the cerebellum. Retrograde tracing data revealed that medium-sized multipolar cells from the magnocellular part of the LRN project to the cochlear nucleus (CN). We sought to characterize the LRN projection to the CN using BDA injections. Anterogradely labeled terminals in the ipsilateral CN appeared as boutons and mossy fibers, and were examined with light and electron microscopy. The terminal field in the CN was restricted to the granule cell domain (GCD), specifically in the superficial layer along the anteroventral CN and in the granule cell lamina. Electron microscopy showed that the smallest LRN boutons formed 1–3 synapses, and as boutons increased in size, they formed correspondingly more synapses. The largest boutons were indistinguishable from the smallest mossy fibers, and the largest mossy fiber exhibited 15 synapses. Synapses were asymmetric with round vesicles and formed against thin dendritic profiles characterized by plentiful microtubules and the presence of fine filopodial extensions that penetrated the ending. These structural features of the postsynaptic target are characteristic of the terminal dendritic claw of granule cells. LRN projections are consistent with known organizational principles of non-auditory inputs to the GCD. J. Comp. Neurol. 504:583–598, 2007.

Indexing terms: auditory; granule cells; mossy fibers; synapse

Multimodal interactions between auditory and traditionally nonauditory structures are well established, but the functional significance of these associations is still being unraveled. Somatosensory information from the cuneate and spinal trigeminal nuclei is conveyed into the auditory system through the cochlear nucleus (CN; Haenggeli et al., 2005; Itoh et al., 1987; Li and Mizuno, 1997; Shore, 2005; Shore et al., 2000; Weinberg and Rustioni, 1987; Wolff and Künzle, 1997; Wright and Ryugo, 1996; Zhou and Shore, 2004). The somatosensory projections originate from those parts of the cuneate and spinal trigeminal nuclei that mediate positional information about the head and pinna. Information about head and pinna position is hypothesized to assist orientation to a sound source in three-dimensional space (Oertel and Young, 2004), because sound spectra are modified by head- and pinna-related transfer functions (Musicant et al., 1990; Rice et al., 1992). The pontine nuclei send sensorimotor projections to the CN, whose function may be to coordinate the tracking of moving sounds (Babalian, 2005; Ohlrogge et al., 2001). The target of these nonauditory projections is the granule cell domain (GCD), a superficial shell region composed primarily of granule cells whose axons terminate in the dorsal cochlear nucleus (DCN) (Mugnaini et al., 1980b).

Many of the inputs to the GCD terminate in the form of mossy fiber endings (Haenggeli et al., 2005; McDonald and Rasmussen, 1971; Mugnaini et al., 1980a; Ohlrogge et al., 2001; Wright and Ryugo, 1996). CN mossy fibers were named for their structural similarity to large endings in the cerebellum. Moreover, the anatomical organization of the GCD within the DCN led to the notion that the DCN

Grant sponsor: National Institutes of Health; Grant number: RO1 DC004395.

*Correspondence to: David K. Ryugo, Center for Hearing and Balance, Johns Hopkins University, 720 Rutland Avenue, Baltimore, MD 21205. E-mail: dryugo@jhu.edu

Received 31 January 2007; Revised 18 June 2007; Accepted 29 June 2007
DOI 10.1002/cne.21463
Published online in Wiley InterScience (www.interscience.wiley.com).

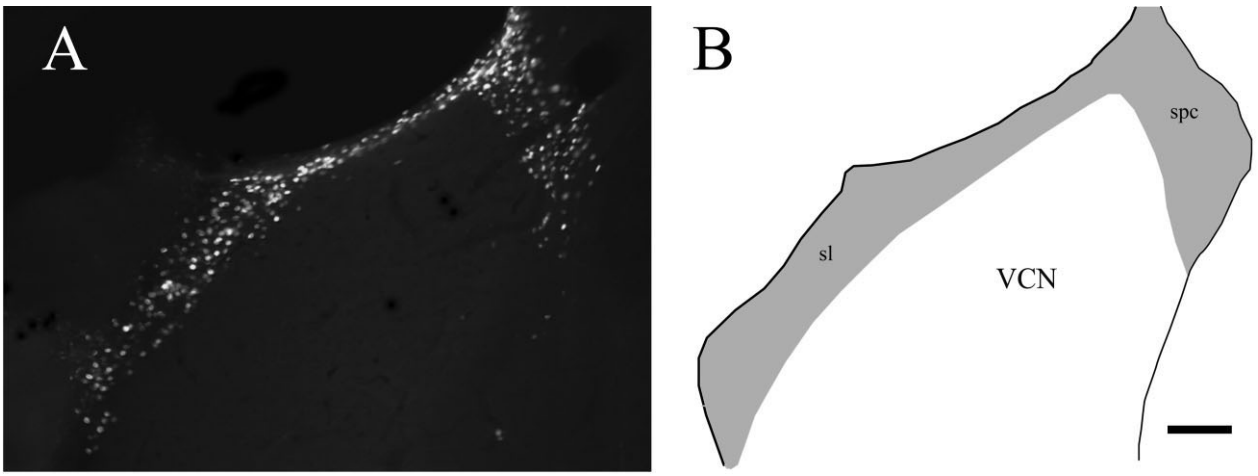

Fig. 1. Photomicrograph (**A**) and drawing (**B**) illustrating the GCD of the CN in the rat. Granule cells were retrogradely labeled by placing an extracellular injection of diamidino yellow in the DCN. The labeled cell bodies form a shell along the lateral, dorsal, and dorsomedial surface of the VCN. This distribution is coincident with the distribution of the GCD as previously described (Mugnaini et al., 1980b) and coincides with the terminal field of projections from the LRN. Abbreviations in this and the other figures are based on the atlas of Paxinos and Watson (1998; see list). Scale bar = 100 μm.

was comparable to a cerebellar folium (Devor, 2000; Lorente de Nó, 1981; Mugnaini et al., 1980a,b; Mugnaini and Morgan, 1987; Wright and Ryugo, 1996). Because structures that supply mossy fibers to the GCD also supply mossy fibers to the cerebellum, we inferred that structures projecting to the cerebellum could also be sources for mossy fiber input to the GCD.

The lateral reticular nucleus (LRN) provides a major mossy fiber input to the deep cerebellar nuclei and cerebellar cortex (Clendenin et al., 1974; Dietrichs and Walberg, 1979; Künzle, 1973, 1975; Matsushita and Ikeda, 1976; Parenti et al., 1996; Ruigrok et al., 1995; Wu et al., 1999). It serves as a nexus for inputs from all levels in the contralateral spinal cord (Künzle, 1973; Menetrey et al., 1983; Rajakumar et al., 1992) and brainstem (Qvist and Dietrichs, 1985, 1986; Walberg et al., 1985). The relationship of high cervical spinal nerves to the LRN (Künzle, 1973) is of special interest because C2 spinal nerves project to the GCD (Zhan et al., 2006) and because activity in C2–C3 modulated the responses of DCN projection neurons (Kanold and Young, 2001). The collective evidence, albeit circumstantial, led us to hypothesize a projection from the LRN to the CN.

Injections of fast blue into the CN were predicted to produce retrogradely labeled cell bodies in the LRN. Although retrograde tracing methods reveal the somatic and sometimes dendritic structure of cells that initiate the projection, they do not provide information regarding structural details of axon branching, sizes and shapes of endings, or postsynaptic targets, because the injection site obscures the field. For such information, we injected biotinylated dextran amine (BDA) into the LRN to examine the anterogradely labeled fibers and endings. Cell bodies labeled by fast blue in the cuneate, spinal trigeminal, and pontine nuclei served as positive retrograde controls (Haenggeli et al., 2005; Ohlrogge et al., 2001; Wright and Ryugo, 1996), and mossy fibers

Abbreviations

ANr	auditory nerve root
AVCN	anteroventral cochlear nucleus
CF	climbing fibers
CN	cochlear nucleus
contra	contralateral
Cu	cuneate nucleus
C1/A1	adrenaline cells
CVRG	caudoventral respiratory group
CVL	caudal ventrolateral reticular nucleus
D, DCN	dorsal cochlear nucleus
ECu	external cuneate nucleus
4th V	4th ventricle
GCD	granule cell domain
gcl	granule cell lamina
Gi	gigantocellular reticular nucleus
GiV	gigantocellular reticular nucleus, ventral division
ICP	inferior cerebellar peduncle
IO	inferior olive
ipsi	ipsilateral
IRt	intermediate reticular nucleus
LRN	lateral reticular nucleus
LRtS5	lateral reticular nucleus, subtrigeminal division
LRtPC	lateral reticular nucleus, parvocellular division
LPGi	paragigantocellular reticular nucleus
MdV	dorsal medullary reticular nucleus, ventral part
MF	mossy fiber
Ml	medial lemniscus
NA	nucleus ambiguus
P, PVCN	posteroventral cochlear nucleus
PT, Py	pyramidal tract
Ro	nucleus of Roller
RVRG	rostral ventral respiratory group
RVL	rostroventrolateral reticular nucleus
sl	superficial layer of GCD
sol	nucleus of the solitary tract
spc	subpeduncular corner of the GCD
Sp5	spinal trigeminal nucleus
Sp5I	spinal trigeminal nucleus, interpolaris division
VCN	ventral cochlear nucleus
VNr	vestibular nerve root
12	hypoglossal nucleus
12n	hypoglossal nerve root

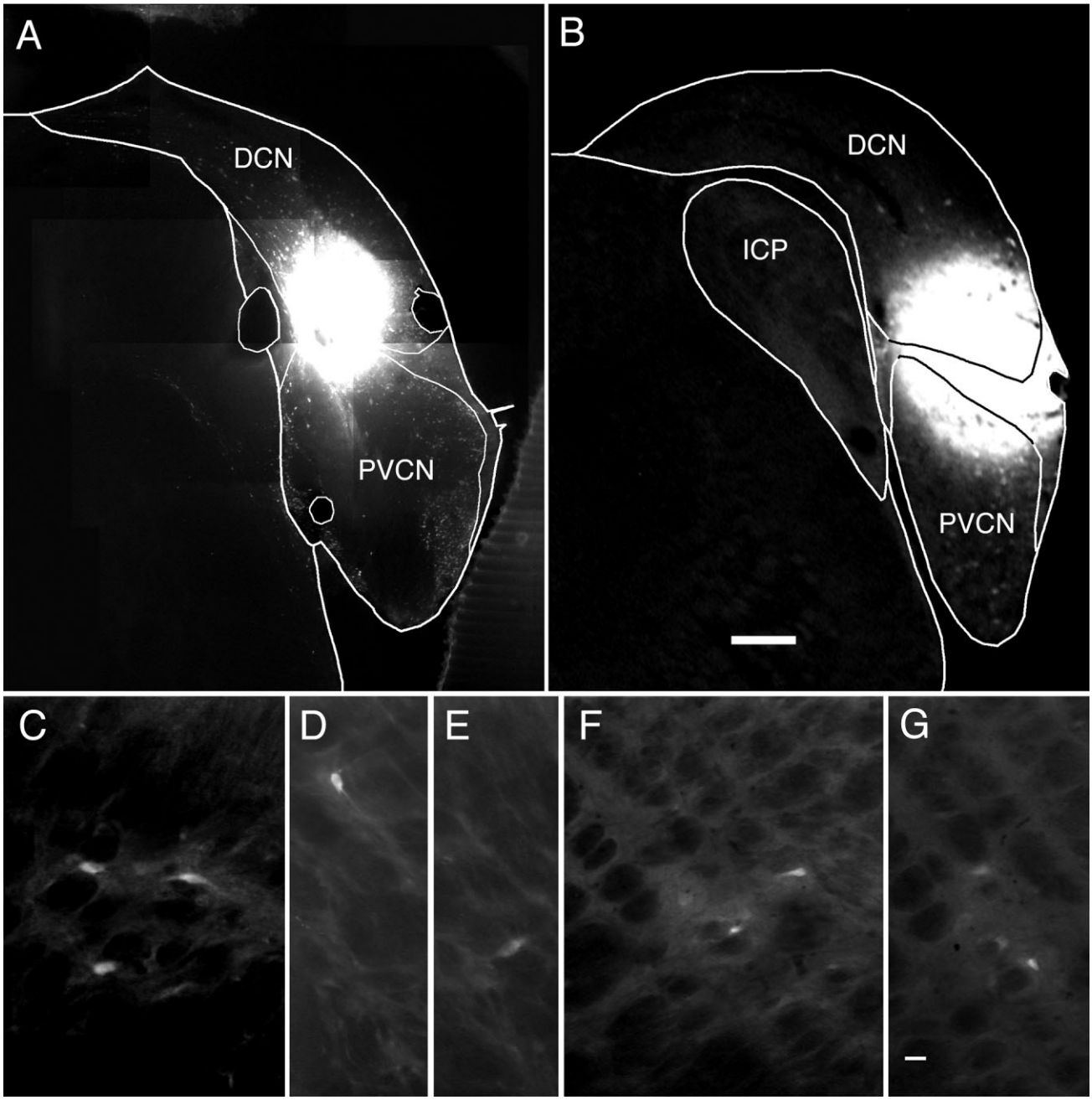

Fig. 2. Photomicrographs of two representative injections of fast blue into the CN (**A,B**). Injections were centered on the granule cell lamina that separates the DCN from the PVCN. Note that the spread of dye is confined within the nucleus. Retrogradely labeled cell bodies (**C–G**) were found in the magnocellular division of the ipsilateral LRN. Scale bars = 0.5 mm in B (applies to A,B); 20 μm in G (applies to C–G).

labeled by BDA in the cerebellum served as positive anterograde controls (Wu et al., 1999). We addressed the following questions. 1) Which division of the LRN gives rise to the axon projections to the CN? 2) Where is the terminal field of the LRN in the CN? 3) What is the structure of the presynaptic ending? 4) What are the postsynaptic targets? Some of these data were presented at the midwinter meeting of the Association for Research in Otolaryngology, New Orleans, February, 2005.

MATERIALS AND METHODS

Twenty-seven rats (270–490 g) were anesthetized by intraperitoneal injection of sodium pentobarbital (45 mg/kg body weight), which was supplemented with addi-

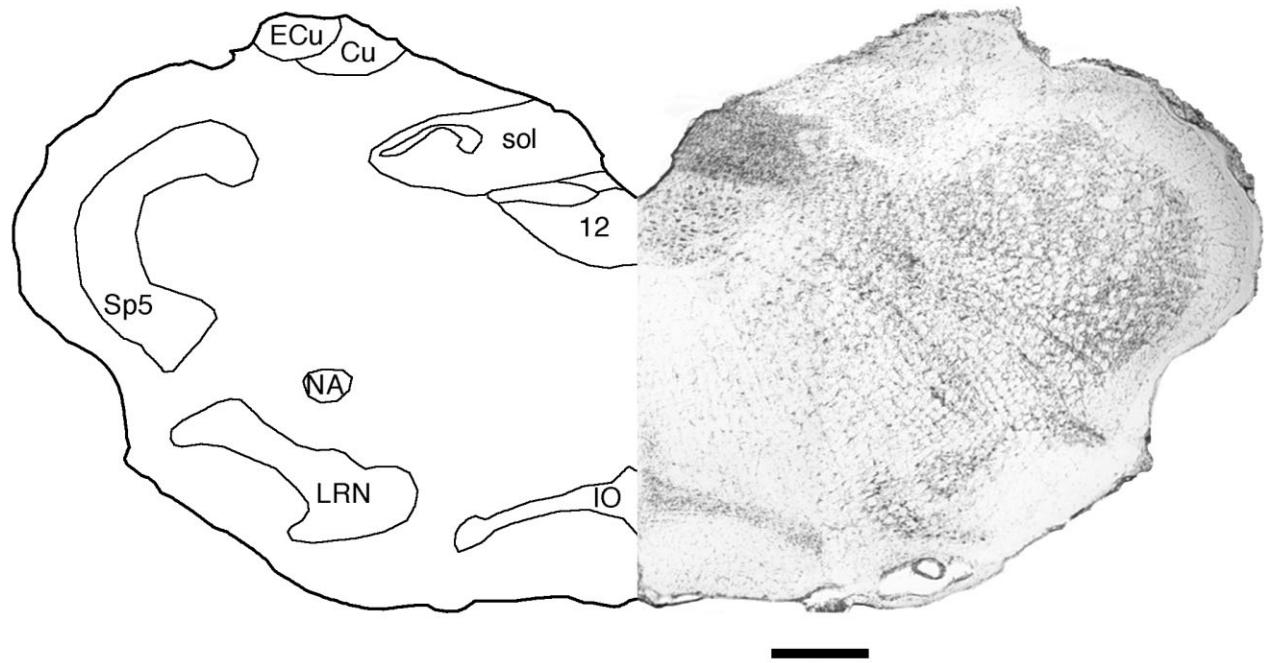

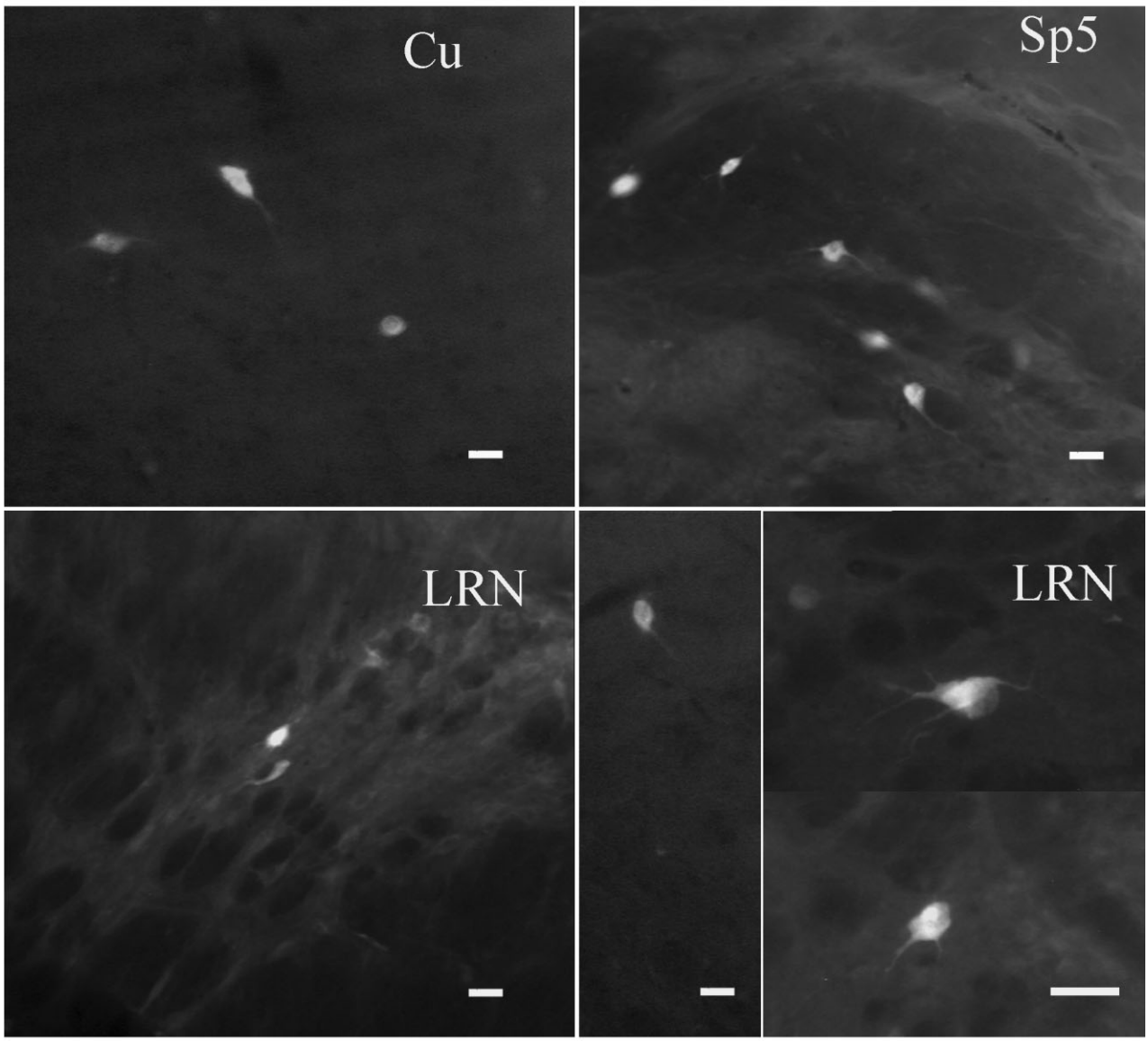

Figure 3

tional doses of ketamine/xylazine when needed. Atropine (0.02 cc, IM) was administered to control secretions. Procedures were initiated only after animals were areflexic to tail or paw pinches. Anesthetized animals were positioned in a headholder, and stereotaxic coordinates (Paxinos and Watson, 1998) were empirically corrected on the basis of subject size. All procedures were performed in accordance with NIH guidelines and approved by the Johns Hopkins University Committee on Animal Care and Use.

CN injections

Six rats were used for CN injections. The posterior fossa was opened by drilling, and the cerebellum was aspirated until the surface of the DCN could be observed. Placement of the electrode tip was made with the rat fixed in a stereotaxic frame using standard ear bars and the incisor bar set at 4.2 mm. The electrode carrier was tilted back in the parasagittal plane 60° from vertical and 24.5° to the side. The pipette (20 μm tip, I.D.) was advanced 1.6–1.8 mm from the DCN surface. Fast blue (Polysciences, Warrington, PA) dissolved in physiological saline (1% w/v) was injected in two 50.6-nl aliquots 10 minutes apart (Nanoject II; Drummond Scientific Co., Broomall, PA).

LRN injections

Twenty-one rats were used for LRN injections. Following a midline incision over the occipital bone, skin and musculature were separated by blunt dissection and the foramen magnum enlarged using rongeurs. With guidance by stereotaxic coordinates, the brainstem was penetrated at 30° off vertical within a parasagittal plane 1.2–1.6 mm lateral to the midline with a glass micropipette (2–10 μm I.D.). The pipette was filled with a 10–15% solution of BDA (Molecular Probes, Eugene, OR) in 0.01 M phosphate-buffered saline (PBS). Tip diameter was verified after each injection. At a predetermined spot, a small injection of the tracer was delivered by applying positive current of 5 μA delivered (7 seconds on, 7 seconds off) for 15–20 minutes.

The LRN was approached in four rats from a ventral surgical approach in order to reduce contamination by "fibers of passage" artifact caused by tracer leakage as the pipette passes through brain tissue. The animal was held in the stereotaxic frame with its ventral surface upward. An incision was made just lateral to the larynx. The skin and neck musculature were separated to expose the base of the occipital bone, and a hole was drilled 2 mm off the midline. The pipette was positioned and advanced with references to the midline and blood vessels. Injection parameters were the same as for the dorsal approach.

At the end of each injection, the skin was sutured, and the rat recovered from anesthesia. After a survival time of 5–9 days, rats were deeply anesthetized with an overdose of sodium pentobarbital (90 mg/kg body weight). The chest cavity was opened, and 0.05 cc of heparin sulfate was injected into the ventricle. The animal was transcardially perfused with 10 cc of 0.12 M PBS with 0.5% sodium nitrite followed immediately by 300 cc of chilled fixative (4% paraformaldehyde in 0.12 M PB). Dissected brains were kept in the same fixative for 1–2 hours, embedded in gelatin-albumin hardened with paraformaldehyde, and cut in transverse sections on a Vibratome (60 μm thickness) through the lower brainstem and cerebellum. Serial sections were collected in culture wells in 0.12 M PB (pH 7.4). Tissue with the fluorescent dye was mounted on gelatin-coated microscope slides, coverslipped with Krystalon, and studied with a fluorescent microscope.

Tissue with the anterograde dye was processed with biotinylated peroxidase-avidin complex (ABC Elite; Vector, Burlingame, CA). Sections were permeabilized by the addition of 0.05% Photo-Flo (Kodak) to ABC solution. Visualization of the BDA was achieved by reacting sections with a solution containing 0.0125% diaminobenzidine-HCl, 0.25% nickel ammonium sulfate, and 0.35% imidazole in 0.05 M cacodylate, pH 7.2. Sections were mounted on gelatin-coated microscope slides, counterstained with cresyl violet, and coverslipped with Permount.

Light microscopic analysis

Injection sites. Photomicrographs were collected that spanned the rostral-caudal extent of each injection site. With the magic wand tool in Adobe Photoshop 7 (Adobe Systems Inc., San Jose, CA), everything above the 75th percentile in density was selected and defined as the core. The core was outlined by drawing a perimeter around what was selected, and then anterior-posterior length and medial-lateral width dimensions were measured. The region immediately surrounding the core between the 50th and the 75th percentiles in density was defined as the halo. Structural boundaries were drawn with a light microscope (total magnification ×30) and computer software (Neurolucida; Microbrightfield, Essex, VT) on the basis of qualitative cytoarchitectural distinctions that were guided by a rat atlas (Paxinos and Watson, 1998).

Projections. The location of retrogradely labeled cell bodies and the course and distribution of anterogradely labeled axons and terminals were studied with a light microscope and plotted using Neurolucida at a total magnification of ×300. Swellings were drawn slightly thicker than scale for clarity. The GCD in CN was highlighted (Fig. 1) according to previously described criteria (Mugnaini et al., 1980b). The LRN was located in counterstained tissue sections and identified by criteria previously published (Kalia and Fuxe, 1985; Kapogianis et al., 1982a,b). Because of relatively sparse labeling of the anterograde projections, maps were created by combining data from pairs of adjacent sections. These plots allowed for the superimposition of the projections onto brainstem structures (Paxinos and Watson, 1998). Projections were followed from the injection site to their terminations in the CN and cerebellum and then photographed. A list of abbreviations is provided.

Electron microscopic analysis

Tissue from six rats with the BDA injection site restricted to the LRN was further prepared for electron

Fig. 3. **Top:** Schematic drawing (left) and photomicrograph (right) through the LRN in coronal section. **Bottom:** Photomicrographs of retrogradely labeled cell bodies from a CN injection. Labeled neurons in the cuneate and spinal trigeminal nuclei served as positive controls. Most labeled neurons in the LRN appeared as multipolar neurons in the magnocellular division of the nucleus. Scale bars = 1 mm at top; 25 μm at bottom.

TABLE 1. Summary of Animals, Injection Sites in the Medullary Reticular Nucleus and Distribution of Labeled Mossy Fibers in Cerebellum and Cochlear Nucleus[1]

Case ID	Locations of injection core in the medullary reticular nucleus and lateral inferior olive	Distribution of the labeled endings			
		Cerebellum		Cochlear nucleus	
		MF	CF	Ipsi-	Contra-
100903b[2]	IO/GiV	–	+	+	+
081602b	Lateral IO/MdV	+	+	+	+
040102a	Lateral IO	+	+	+	+
050902a	Lateral IO	+	+	+	+
050902b	Lateral IO	+	+	+	–
052302a	Lateral IO	+	+	+	–
031302a	LRN/MdV	+	–	+	+
032202b	LRN/LPGi	+	–	+	+
100903c[2]	LRN	+	–	+	–
120203c[2]	LRN	+	–	+	–
011804a[2]	LRN	+	–	+	–
051606b	LRN/LPGi	+	–	+	–
052906	LRN	+	–	+	–
053006a	LRN	+	–	+	–
061506a	LRN	+	–	+	+
061506b	LRN	+	–	–	–
070506a	LRN	+	–	+	–
070506b	LRN	+	–	+	+
072106a	LRN	+	–	+	–
072106b	LRN	+	–	+	+
070606a	LRN	+	–	+	–

[1]+, Labeled endings observed; –, no labeled endings. observed.
[2]Ventral approach.

microscopic analysis. Tissue sections containing labeled axons, boutons, and mossy fiber endings were treated with 1% osmic acid (15 minutes), stained en bloc with 1% uranyl acetate overnight, dehydrated, and embedded in Polybed 812. Selected regions from the GCD were excised and reembedded in BEEM capsules for ultrathin sectioning. Light microscopic maps of these smaller blocks were made for orientation purposes, using blood vessels and labeled structures as landmarks, so that the endings of interest could be found in the electron microscope. A series of consecutive ultrathin sections (up to 90 sections) was collected on Formvar-coated slotted grids. Sections were studied and photographed with a Hitachi H-7600 electron microscope.

Digital imaging

Photomicrographs were collected using a color chilled 3CCD Hamamatsu C5810 camera (Hamamatsu, Hamamatsu City, Japan) or an Optronics MicoFire digital camera (Optronics, Goleta, CA) attached to light microscopes. Electron micrographs were collected by using an AMT-XR-100 bottom mount (1,000 × 1,000) CCD camera (Advanced Microscopy Techniques, Danvers, MA). Images were opened, minimally modified, and stored with Photoshop 7.0. Fluorescent micrographs were not altered. Brightfield micrographs were matched with each other by changing brightness but otherwise were not altered. Electron micrographs were balanced with each other only in terms of brightness and contrast.

RESULTS

The results of this study are based on retrograde and anterograde labeling data demonstrating a neural circuit between the LRN and the CN. Localized, unilateral injections of fast blue were confined to the CN and observed to encroach upon the granule cell lamina (Fig. 2). In each of these six cases, 8–22 retrogradely labeled cell bodies were found in the ipsilateral LRN. Fast blue marked the cell body and short lengths of the primary dendrites (Fig. 3). The shapes of the cell bodies varied from fusiform to polygonal. Primary dendrites sometimes hinted at a bipolar shape, but in general the dendrites were mostly suggestive of multipolar neurons. There was not, however, sufficient detail to afford definitive cell type identification as defined by Golgi stain criteria (Kapogianis et al., 1982b). Labeled cells were distributed in the magnocellular division of the LRN; they were not found in the parvocellular or subtrigeminal divisions.

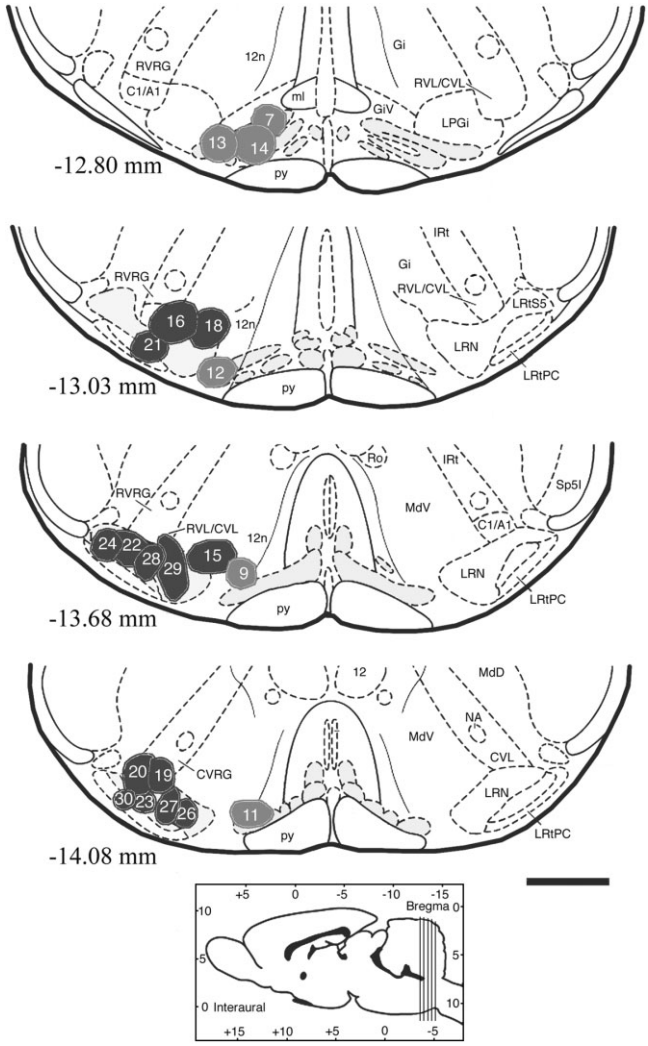

Fig. 4. Plot of injection sites in all cases aimed at the LRN and presented in this report. The injections involved different subdivisions of the reticular nucleus, including the LRN, LPGi, and MdV. The injection cores are indicated by animal number and were reconstructed with the aid of a light microscope and drawing tube, scaled, and assigned to standard atlas sections on the basis of brainstem landmarks (Paxinos and Watson, 1998). The core of injection sites that encroached upon the main LRN is indicated by dark figures, whereas those upon the inferior olive are indicated by light figures. Each injection site is numbered (Table 1), and each section is presented with Bregma coordinates at lower left. A parasagittal view is also shown that indicates the position of the coronal sections (**inset**). Scale bar = 1 mm.

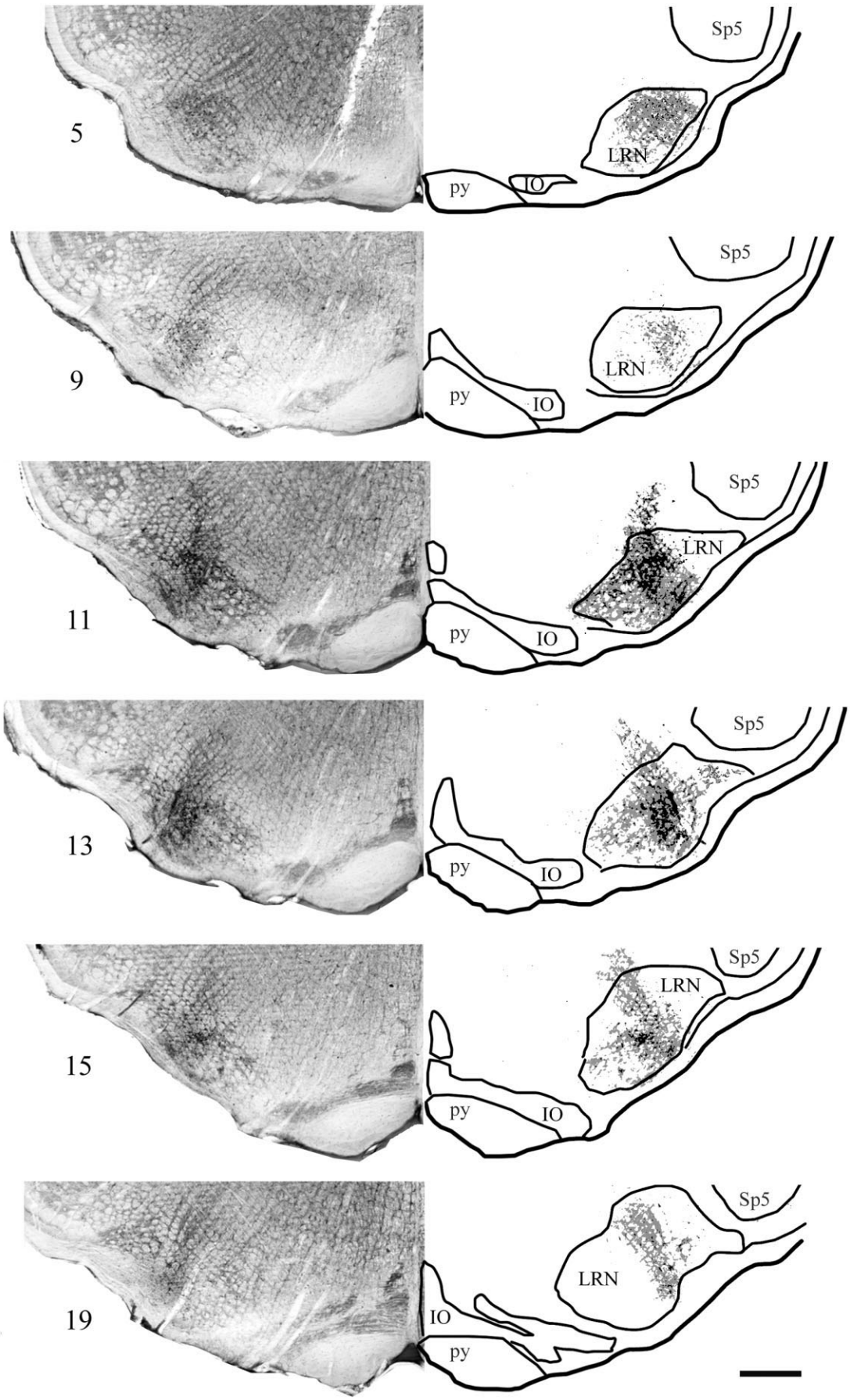

Fig. 5. Photomicrographs (**left**) and drawings (**right**) of a representative injection site in the LRN. The BDA reaction product was "thresholded," copied, flipped horizontally, and pasted onto the drawing. Thus the drawings are mirror images of the photomicrographs. The core of the injection is dark, whereas the halo is a lighter gray. The section numbers are indicated separately, progressing from caudal (5) to rostral (19). Scale bar = 0.5 mm.

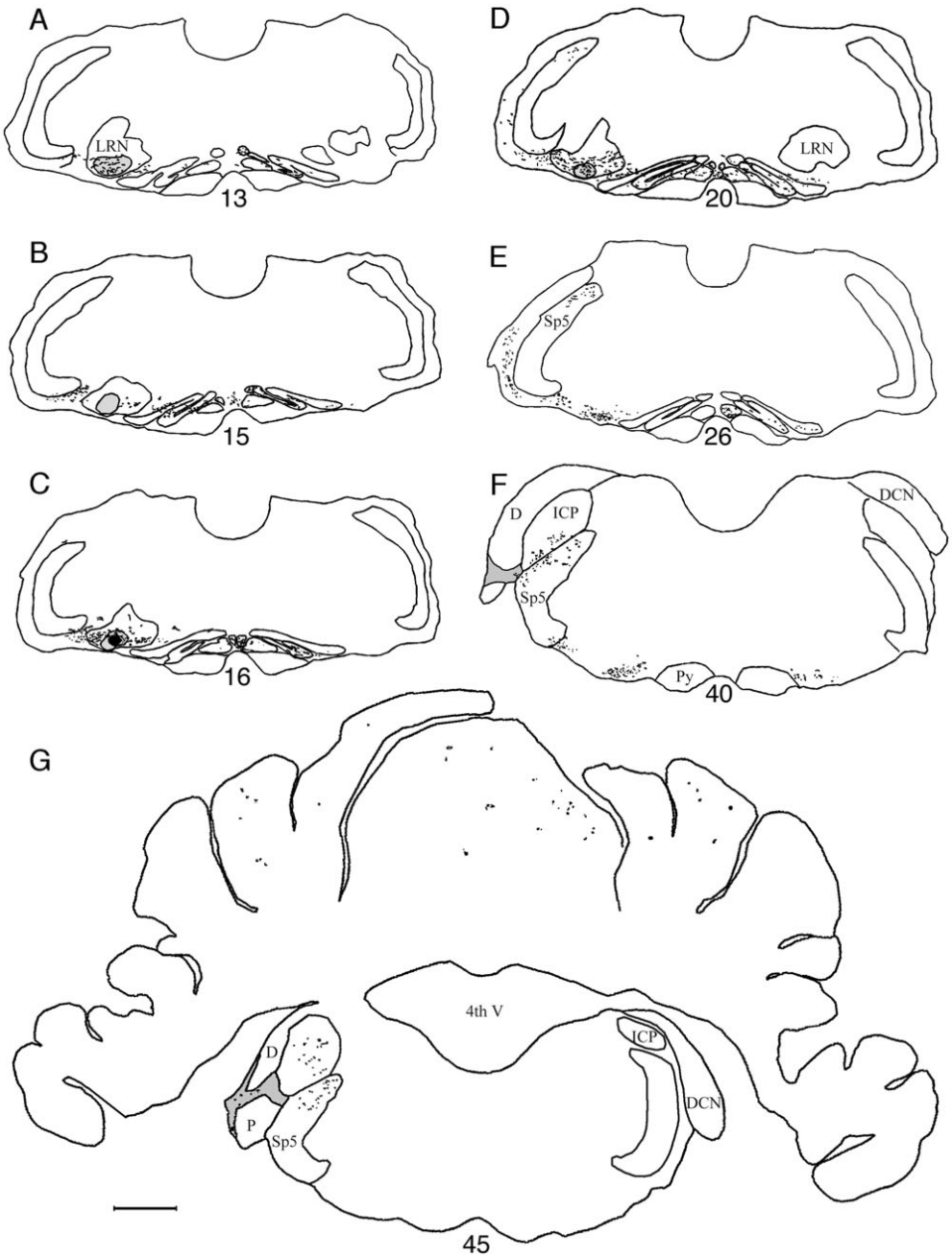

Fig. 6. **A–G:** Plots of the anterograde projection from the LRN to the ipsilateral CN through coronal sections (case 070506a). The injection site core is indicated in black (C), and the halo is indicated in light gray (**A–D**). The labeled swellings and axon segments are drawn as dots and dashes, respectively. The terminal field is located within the GCD (gray in F,G) of the CN. The number of each section is indicated, progressing from caudal (13) to rostral (45). Scale bar = 1.0 mm.

The retrograde data guided placement of injections into the ventral medulla of 21 rats (Table 1). These injections resulted in BDA-labeled axons and terminals in the CN. The average (±SD) dimensions of the core of the BDA reaction product at the injection site were determined: the long axis was 457.7 ± 91.7 μm and the perpendicular short axis 365.1 ± 75.8 μm. These injection sites occasionally included the lateral portion of the inferior olive, lying between the descending tract of the trigeminal and the pyramidal tract and caudal to the facial motor nucleus (Fig. 4).

Ascending pathway of the LRN

The anterograde projections of BDA-labeled axons from each injection in the LRN were analyzed and plotted. Photomicrographs through a representative "hit" are shown for the LRN with the injection site and corresponding drawings of the relevant structures (Fig. 5). The core of the injection site (black) and surrounding "halo" (gray) are shown.

Labeled fibers, 2–3 μm in diameter, emerged from the injection site and traveled laterally and rostrally in the ipsi-

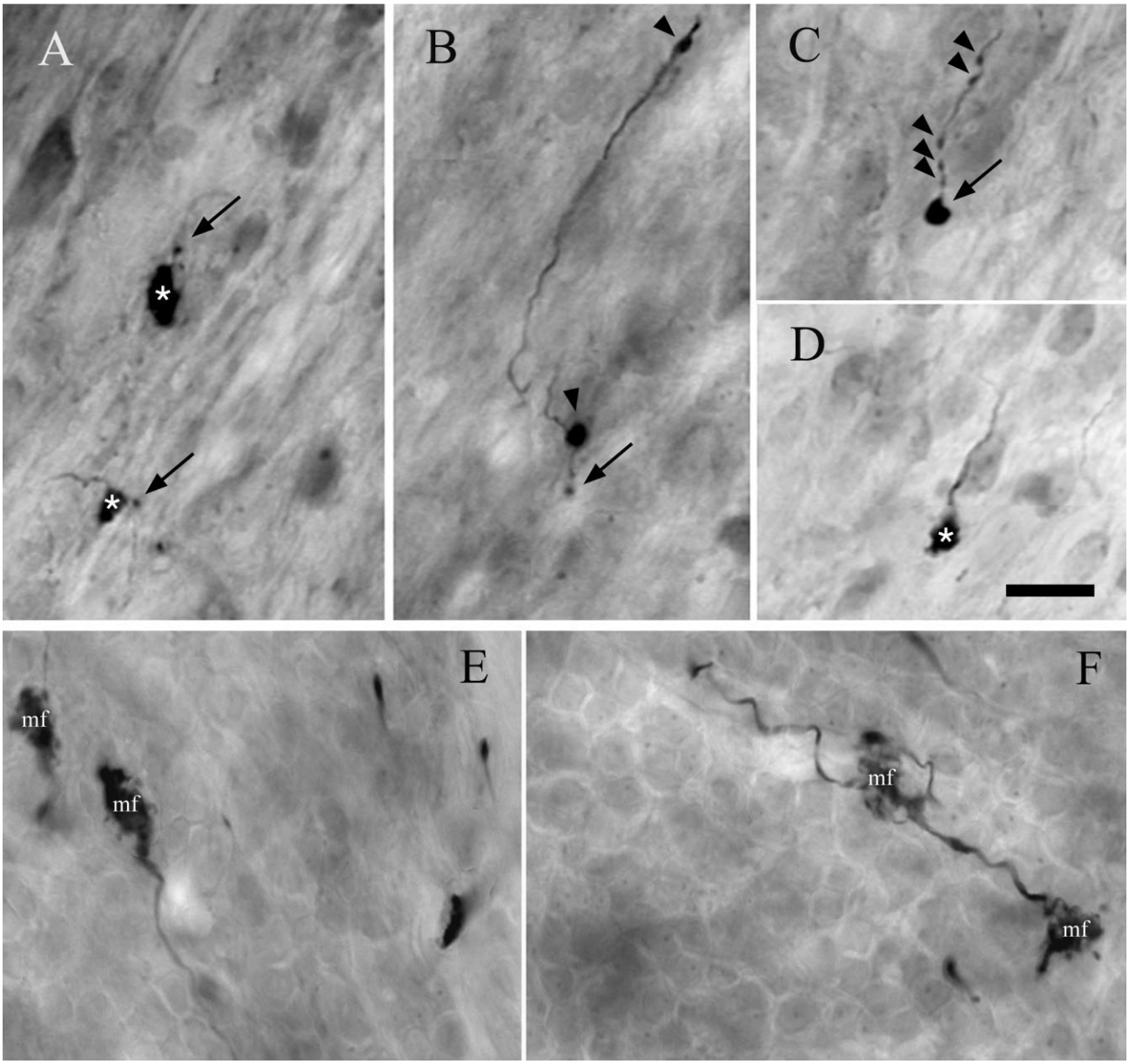

Fig. 7. Photomicrographs show LRN swellings in the CN (**A–D**) and mossy fibers (mf) in the cerebellum (**E,F**). The LRN swellings arise from beaded axons marked by en passant swellings (arrowheads) and give rise to terminal swellings that can be classified into one of two types on the basis of their morphological characteristics. One type is large (asterisks), often emits one or several short filaments (A,B,D), and is called a *mossy fiber*. In contrast, the other type is simply a small swelling (A–C, arrows). Mossy fibers (mf) in the cerebellum are larger and exhibit more complex shapes (E,F), and these serve as positive controls that the injection site was situated in the LRN. Scale bar = 10 μm.

lateral ventral spinocerebellar tract (Fig. 6). There was, however, a small but distinct contralateral projection that passed through the inferior olives on both sides as it traveled rostrally and entered the contralateral ventral spinocerebellar tract. As the fibers ascended the brainstem, they also moved dorsally (Fig. 6F). When they approached the level of the CN, some fibers gave rise to a laterally directed branch that entered the medial sheet of the GCD in the ventral cochlear nucleus (VCN; Fig. 6F). Other fibers entered the inferior cerebellar peduncle and traveled dorsally before giving rise to branches that entered the CN through the intermediate and dorsal acoustic striae (Fig. 6G). Most of the fibers continued on into the cerebellum with collaterals given off to the deep cerebellar nuclei.

CN

The branches entering the CN were thinner (1–2 μm) than the parent fiber (Fig. 7A,B) and passed through the granule cell lamina that separates the DCN from the VCN. The fibers tended to be varicose (Fig. 7B,C), and short branches

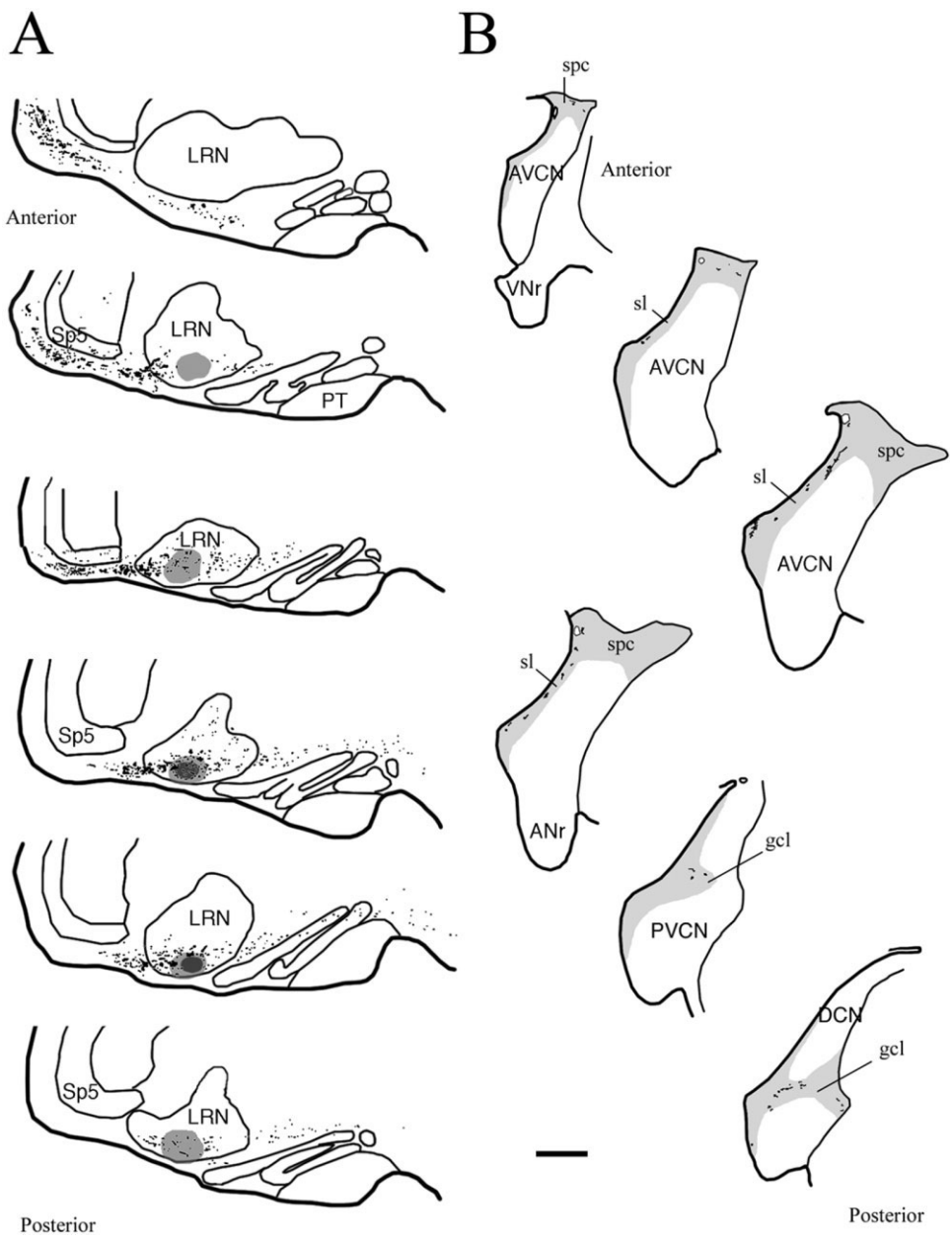

Fig. 8. Plot of axonal trajectory from the injection site (case 053006a) to the CN. **A:** Neurolucida drawings were made of relevant sections that illustrate the injection of BDA in the LRN, and the path of the labeled axons (black dots) as they ascend the brainstem in the ventral spinocerebellar tract. The core of the injection site is indicated in dark gray, and the halo is indicated in lighter gray. **B:** Neurolucida drawings of the distribution of labeled swellings in the CN. The GCD is indicated in gray. The LRN terminal field was reproducible across the animals. Scale bar = 0.5 mm.

formed to terminate in the superficial layer or nearby lamina. These varicosities appeared as small (1–3 μm in diameter) en passant swellings (arrowheads, Fig. 7B,C) or terminal boutons (arrows, Fig. 7A,B,C), and less frequently as larger (4–10 μm in diameter) endings called *mossy fibers* (asterisks, Fig. 7A,D). The mossy fibers of the CN had a diameter three to six times larger than that of boutons, and exhibited relatively smooth profiles. The cerebellar mossy fibers, in contrast, were highly irregular, with twists, branches, and spines (mf; Fig. 7E,F).

The distribution of LRN fiber segments and swellings in the CN was plotted for each animal and a representative case is illustrated in Figure 8A. Fibers ascended in the ventral spinocerebellar tract (Fig. 8B) and arrived at the CN medially at the level of the granule cell lamina. Fibers that penetrated the CN distributed endings within the lamina, the superficial layer, and the subpeduncular corner (Fig. 9). The lamina and superficial layer were the main recipients of LRN projections, and there was no projection into the magnocellular core of the CN where the

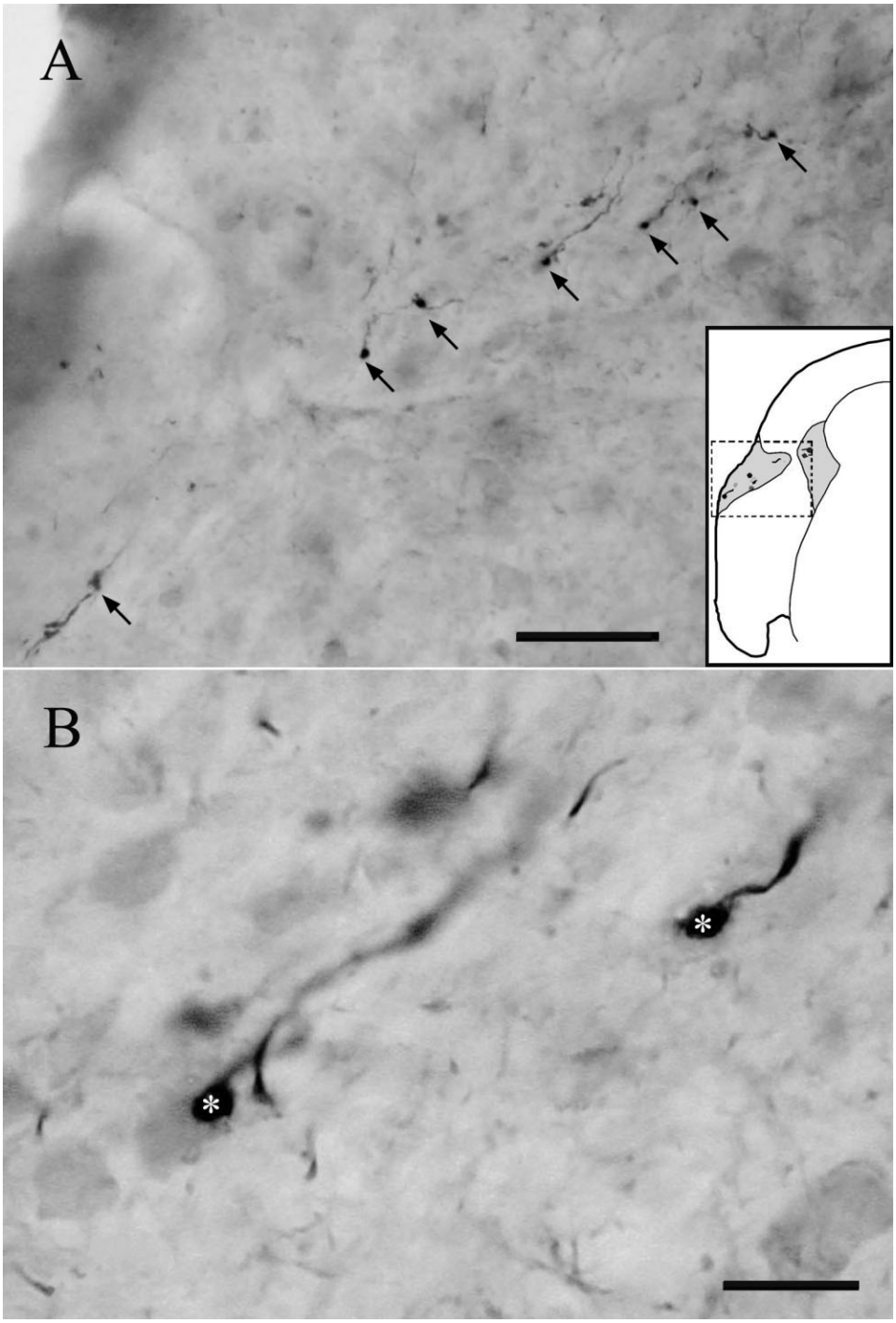

Fig. 9. Photomicrographs of mossy fibers in the lamina of the GCD. **A:** LRN axons give rise to a series of mossy fibers whose position is indicated by the *inset* drawing. **B:** Higher magnification photomicrograph of mossy fibers (asterisks). In the light microscope, these mossy fibers are clearly larger than the bouton endings and exhibit a relatively smooth surface. Scale bars = 50 μm in A; 10 μm in B.

projecting cells reside. The bulk of the labeled fibers continued on in the inferior cerebellar peduncle.

Ultrastructure

Electron microscopy was utilized to verify that the labeled swellings formed true synaptic contact with the resident neurons of the GCD. The two forms of endings, boutons and mossy fibers, were similar in internal structure. The bouton endings were small (<3 μm in diameter), either en passant or terminal, and relatively spherical. They were filled with round synaptic vesicles (45–50 nm diameter), contained centrally placed mitochondria, and formed asymmetric membrane thickenings (Fig. 10). The smallest boutons formed one to three synapses; larger

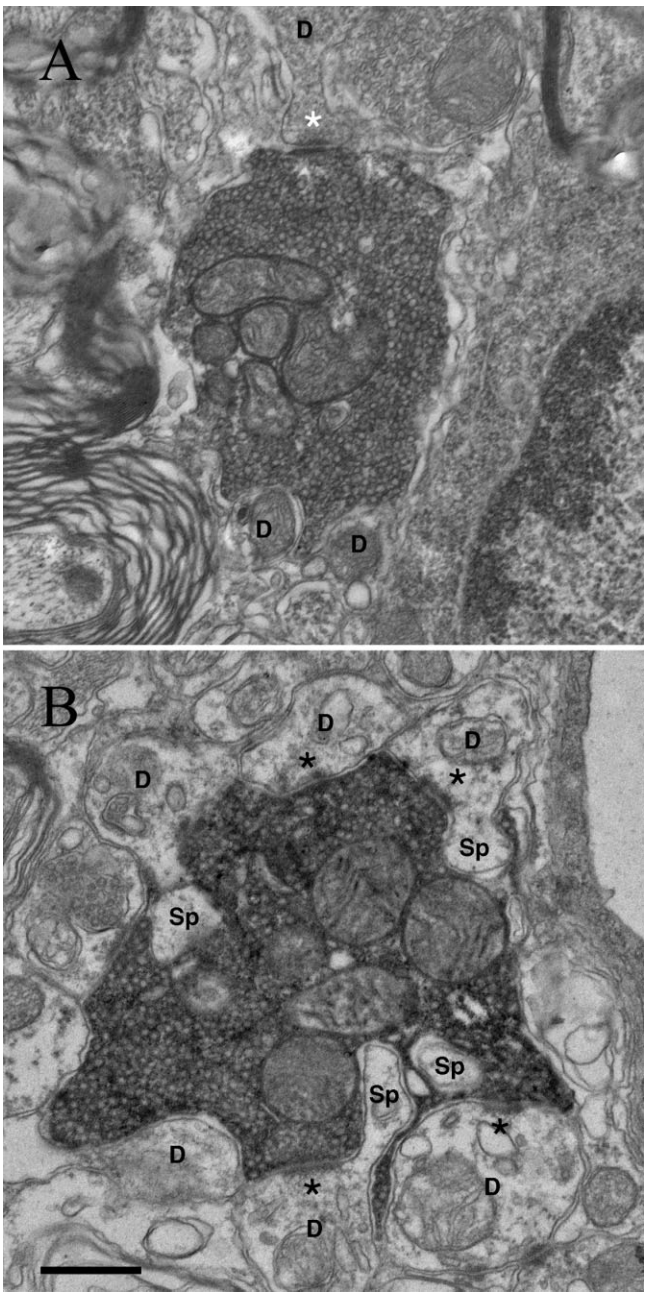

Fig. 10. Electron micrographs illustrate representative bouton endings (**A,B**) in the CN. These endings house a central cluster of mitochondria and are filled with round synaptic vesicles (45–50 nm in diameter). They form asymmetric membrane thickenings (asterisks) with structures that exhibit structural characteristics of the dendrites of granule cells (D). Dendritic spines (Sp) frequently penetrate into the mossy fiber. Scale bar = 0.5 μm.

boutons gave rise to short filopodia and formed proportionally more synapses. Serial section reconstructions of boutons indicated that they formed multiple synapses with thin, pale dendrites. From serial sections, these dendrites were observed to be the termination of straight, unbranched dendritic shafts that contained abundant numbers of microtubules. The terminal dendrites were less than 1 μm in diameter and gave rise to spine-like excrescences that pierced the synaptic ending. The morphology of these dendrites was consistent with that of granule cells where two or three dendritic claws appeared to contact an individual ending.

The larger endings were called *mossy fibers* and were variable in size (4–10 μm in diameter). They were irregular in shape, with a central core (3–6 μm in diameter) and radiating filopodia (Fig. 11). The filopodia were also irregular in shape and of varying thicknesses and lengths. The entire structure was filled with round synaptic vesicles (45–50 nm diameter) and formed asymmetric postsynaptic thickenings (Fig. 11). A single mossy fiber can form up to 15 synapses, and the targets were small, round dendritic profiles. These profiles arose from relatively thin, aspinous dendrites that were smooth and rich in microtubules and mitochondria. When viewed in cross-section, they exhibited round to oval shapes. Dendritic profiles were occasionally observed to fork and form a claw-like structure. In three dimensions, the mossy fiber core and filopodia formed synapses with the terminal dendritic claw, where spines frequently penetrated the presynaptic ending. Each mossy fiber was situated within a nest formed by several dendritic claws.

Cerebellar terminations

The presence of labeled mossy fibers in the deep cerebellar nuclei and cerebellar cortex served as a positive control for injections into the LRN. Cerebellar mossy fibers accompanied all cases with mossy fibers in the CN. The distribution of mossy fibers within the cerebellum was consistent with that previously reported where they were observed in the vermis (lobes IV, V, and VI) and bilaterally in the simple lobe, crus I and II, and paraflocculus of the cerebellar hemispheres (Wu et al., 1999). The rats with the injection core within the LRN had greater numbers of more darkly labeled mossy fibers in the cerebellum compared with those with the injection core on the edge of the LRN. The cerebellar mossy fibers were typically larger than those of the CN (Fig. 7).

Injections outside the LRN

In six cases, the injection cores were located in the lateral aspect of the inferior olive. Ending morphology and the distribution pattern appeared similar to that in the LRN cases, with mossy fibers in the CN and cerebellar cortex. In addition, the cerebellum contained labeled climbing fibers. We inferred that this labeling pattern was caused by tracer uptake by fibers of passage, because a small but distinct fraction of LRN projecting axons cross the midline and pass through the inferior olive to ascend in the spinocerebellar tract (Figs. 6, 8).

DISCUSSION

The results of this anterograde tracing study demonstrate a projection from the LRN to the ipsilateral GCD of the CN, with a minor projection to the contralateral CN. Multipolar cells of the magnocellular division of the LRN appear to be the source of the projection, although we cannot rule out a contribution from fusiform cells. The projection to the CN arises from collaterals off the main projection to the cerebellum. The terminal field in the

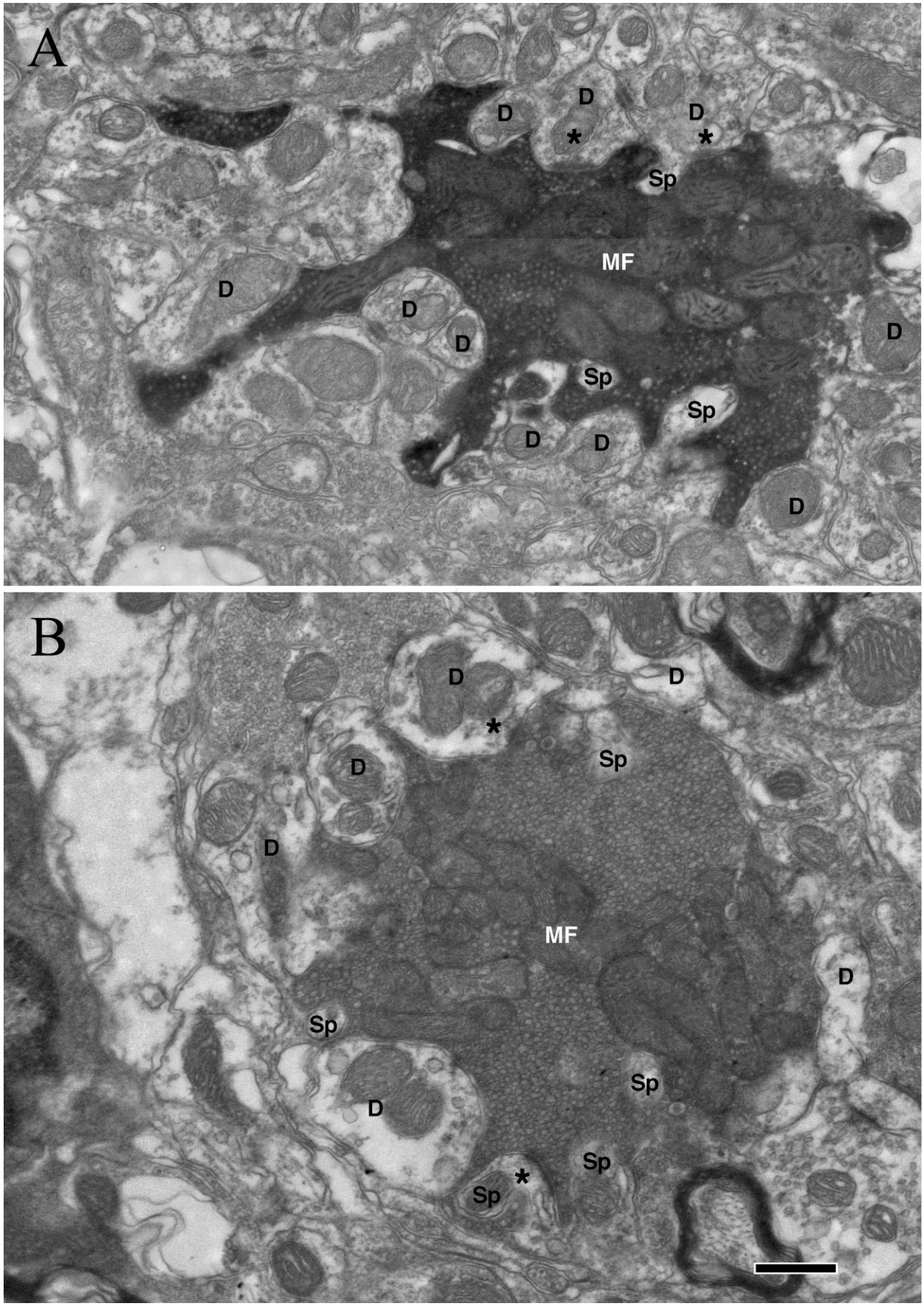

Fig. 11. Electron micrographs illustrate two (**A,B**) representative mossy fiber (MF) endings in the CN. The mossy fibers exhibit a relatively irregular surface, having a central core and radiating branches of variable lengths. The entire structure is filled with round synaptic vesicles (45–50 nm in diameter). The ending itself appears surrounded by round dendritic profiles (D) from which short spines (Sp) protrude. Asymmetric synapses are formed between the mossy fiber and the dendritic structures (asterisks). Scale bar = 0.5 μm.

GCD consists of bouton and mossy fiber endings where asymmetric synapses are formed with what appear to be the dendrites of granule cells.

Technical considerations

Injection sites and retrograde labeling. Fast blue injections into the CN produced bilateral, retrograde labeling of cell bodies in the LRN with a dominant ipsilateral bias. This labeling pattern verified previous results using Fluoro-Gold and diamidino yellow injections into the CN (Ryugo et al., 2003). Fewer LRN cell bodies were labeled in the present study, but this result likely is due to smaller injections that completely avoided the inferior cerebellar peduncle. The variation could also be due in part to differences in tracer chemistry and intracellular transport. A comparison among these dyes likewise resulted in fewer fast blue-labeled cell bodies in the pontine, cuneate, and spinal trigeminal nuclei, although it is known that these nuclei give rise to robust projections to the CN (Haenggeli et al., 2005; Ohlrogge et al., 2001; Weinburg and Rustioni, 1987; Wright and Ryugo, 1996; Zhou and Shore, 2004).

Projection patterns. BDA has proved itself a sensitive neuronal tracer by revealing collateral projections in axons (Chen and Aston-Jones, 1998). Details regarding the LRN-cerebellum circuit were expanded by the demonstration of LRN collaterals to the deep cerebellar nuclei and multiple folia of the cerebellum (Wu et al., 1999). LRN projections to any single location are modest because of the widespread distribution of the collaterals, so this situation may explain why the use of retrograde tracers such as fast blue and Fluoro-Gold in the cerebellar cortex yielded only a modest number of labeled bodies in the LRN. These kinds of results emphasize the need to employ anterograde and retrograde tracing methods as well as different types of dyes when studying connectivity within the central nervous system.

Contamination by fibers of passage. The LRN is surrounded by structures that potentially contribute mossy fibers to the cerebellum. Both ventral and dorsal approaches to the LRN were used to control for accidental BDA uptake as the dye-filled pipette passed through the tissue. Specifically, we sought to avoid contamination by fibers of the C2 dorsal root ganglion that project to the CN (Zhan et al., 2006). It was also important to avoid fibers of the cuneate and spinal trigeminal nuclei or other potential sources of input. A consistent labeling pattern in the GCD emerged in spite of the different approaches to the LRN, suggesting that contamination by nonspecific fibers of passage had been controlled. In addition, we observed labeled LRN projections crossing through the inferior olives on both sides. This observation shows that injections of an anterograde tracer in the inferior olive could label fibers originating in the LRN. On the basis of these anterograde data, the inferior olive was eliminated as a source of input to the CN. This interpretation was consistent with the lack of retrograde cell labeling in the inferior olive when CN injections were completely confined to the CN.

Projections from the LRN to CN

Our results showed that the terminals from the LRN appeared exclusively in the GCD of the CN. The GCD has been implicated as an integrative center in the CN (Oertel and Young, 2004). It contains a multitude of microneurons whose local circuit projections terminate on the principal projection neurons of the DCN (Manis, 1989; Mugnaini et al., 1980b) and is well situated to influence ascending auditory information. This influence is presumably mediated by the nonauditory inputs from somatosensory, vestibular, sensorimotor, and aminergic systems (Behrens et al., 2002; Haenggeli et al., 2005; Newlands and Perachio, 2003; Ohlrogge et al., 2001; Shore, 2005; Wright and Ryugo, 1996; Ye and Kim, 2001; Zhan et al., 2006; Zhou and Shore, 2004). The general function of these inputs could involve arousal level and proprioceptive feedback that are integrated to locate and identify sound sources. The aminergic systems could set the "gain" of CN output. The utility of proprioceptive sensations could be to monitor stationary sounds when the organism is moving or to track a moving object when the animal is stationary.

Although we did not reconstruct a dendritic claw back to its granule cell body of origin for this study, the structural features of the dendrites were consistent with those of granule cells (Weedman and Ryugo, 1996). Other cells of the GCD are unipolar brush cells, chestnut cells, and Golgi cells. The dendrites of unipolar brush cells and their synaptic relationships with mossy fibers are morphologically distinct (Weedman et al., 1996). Chestnut cells do not have dendrites but receive mossy fibers on their somata (Weedman et al., 1996). The fine structure of dendrites of Golgi cells in the CN have not been described. The consistent synaptic relationship of labeled endings with thin, spiny terminal dendrites across a broad region of the GCD and the sheer number of observations implicate granule cells in this relationship. The output of the granule cells is to the molecular layer of the DCN (Mugnaini et al., 1980b), where they deliver multimodal information to the apical dendrites of pyramidal cells that represent the main output of the nucleus (Manis, 1989). In this way, the LRN can affect acoustic information processing.

Possible significance of projections

The auditory system has classically been regarded as being composed of neural structures that are connected directly or indirectly to the cochlea. For sound to have meaning, however, it must have significance beyond the simple stimulus parameters of spectral content, level, and location. The processing of sound should therefore involve additional neural systems that have not been historically considered "auditory." The LRN has emerged as a structure that could influence acoustic processing because of its connections with a variety of sensory systems. Three possible functions of the LRN in auditory processing are considered in light of our current results.

First, the LRN receives projections from C3 and C4 spinal nerves (Künzle, 1973; Mizuno and Nakamura, 1973). The peripheral processes of these cervical sensory nerves innervate neck, shoulder, and forelimb muscles, and their inputs signal movement of the head relative to the forelimbs and body (Ezure and Tanaka, 1997; Maki and Furukawa, 2005; Rao and Ben-Arie 1996; Yates and Stocker, 1998). Stimulation of spinal nerve C2–C3 produced responses in the principal cells of the DCN, presumably conveying information about head-related transfer functions and sound directionality (Kanold and Young, 2001; Musicant et al., 1990; Rice et al., 1992). Postural data (Flumerfelt et al., 1982; Künzle, 1973; Shokunbi et al., 1985) would complement information regarding pinna orientation (Kanold and Young, 2001), eye

direction (Qvist and Dietrichs, 1985, 1986), and body position with respect to gravity (Newlands and Perachio, 2003; Walberg et al., 1985). The integration of this collective sensory information could serve to stabilize and orient the body with respect to auditory, vestibular, and visual space.

Second, the LRN receives spinal input from visceral receptors that are thought to integrate cardiovascular and respiratory functions (Babic and Ciriello, 2004; Ezure and Tanaka, 1997; Macron et al., 1985; Shintani et al., 2003; Stocker et al., 1997). These studies have suggested autonomic influences on somatic motor activity (Yates and Stocker, 1998). Autonomic projections might also form the afferent limb of reflexes that suppresses auditory sensitivity to self-generated noises made by heartbeats, blood flow, and breathing. The suppression of internal noise is clearly different from the suppression of self-vocalizations that involve the spinal trigeminal nucleus (Haenggeli et al., 2005; Shore, 2005)

Third, the LRN could have a role in vocalizations because of its involvement in respiratory activity (Jurgens, 2002). Vocalization is a complex behavior, the production of which involves the larynx, respiratory movements, and articulators. Vocal tract structure and respiration are influenced by the LRN; proper vocalization also requires feedback from the auditory system (Egnor et al., 2006). On the basis of comparing vocal memories with vocalization feedback, the vocal motor system can compensate and make corrections to optimize communication. In short, our anatomical findings could contribute to understanding any or all of these circuits.

ACKNOWLEDGMENTS

The authors thank Karen Montey and Tan Pongstaporn for technical assistance and Christa Baker for critical reading of the manuscript.

LITERATURE CITED

Babalian AL. 2005. Synaptic influences of pontine nuclei on CN cells. Exp Brain Res 167:451–457.

Babic T, Ciriello J. 2004. Medullary and spinal cord projections from cardiovascular responsive sites in the rostral ventromedial medulla. J Comp Neurol 469:391–412.

Beherns EG, Schofield BR, Thompson AM. 2002. Aminergic projections to cochlear nucleus vias descending auditory pathways. Brain Res 955: 34–44.

Chen S, Aston-Jones G. 1998. Axonal collateral–collateral transport of tract tracers in brain neurons: false anterograde labelling and useful tool. Neuroscience 82:1151–1163.

Clendenin M, Ekerot CF, Oscarsson O, Rosen I. 1974. Distribution in cerebellar cortex of mossy fibre afferents from the lateral reticular nucleus in the cat. Brain Res 69:136–139.

Devor A. 2000. Is the cerebellum like cerebellar-like structures? Brain Res Rev 34:149–156.

Dietrichs E, Walberg F. 1979. The cerebellar projection from the lateral reticular nucleus as studied with retrograde transport of horseradish peroxidase. Anat Embryol 155:273–290.

Egnor SE, Iguina CG, Hauser MD. 2006. Perturbation of auditory feedback causes systematic perturbation in vocal structure in adult cotton-top tamarins. J Exp Biol 209:3652–3663.

Ezure K, Tanaka I. 1997. Convergence of central respiratory and locomotor rhythms onto single neurons of the lateral reticular nucleus. Exp Brain Res 113:230–242.

Flumerfelt BA, Hrycyshyn AW, Kapogianis EM. 1982. Spinal projections to the lateral reticular nucleus in the rat. Anat Embryol 165:345–359.

Haenggeli CA, Pongstaporn T, Doucet JR, Ryugo DK. 2005. Projections from the spinal trigeminal nucleus to the cochlear nucleus in the rat. J Comp Neurol 484:191–205.

Itoh K, Kamiya H, Mitani A, Yasui Y, Takada M, Mizuno N. 1987. Direct projections from the dorsal column nuclei and the spinal trigeminal nuclei to the cochlear nuclei in the cat. Brain Res 400:145–150.

Jurgens U. 2002. Neural pathways underlying vocal control. Neurosci Biobehav Rev 26:235–258.

Kalia M, Fuxe K. 1985. Rat medulla oblongata. I. Cytoarchitectonic considerations. J Comp Neurol 233:285–307.

Kanold PO, Young ED. 2001. Proprioceptive information from the pinna provides somatosensory input to cat dorsal cochlear nucleus. J Neurosci 21:7848–7858.

Kapogianis EM, Flumerfelt BA, Hrycyshyn AW. 1982a. Cytoarchitecture and cytology of the lateral reticular nucleus in the rat. Anat Embryol 164:229–242.

Kapogianis EM, Flumerfelt BA, Hrycyshyn AW. 1982b. A Golgi study of the lateral reticular nucleus in the rat. Anat Embryol 164:243–256.

Künzle H. 1973. The topographic organization of spinal afferents to the lateral reticular nucleus of the cat. J Comp Neurol 149:103–115.

Künzle H. 1975. Autoradiographic tracing of the cerebellar projections from the lateral reticular nucleus in the cat. Exp Brain Res 22:255–266.

Li H, Mizuno N. 1997. Single neurons in the spinal trigeminal and dorsal column nuclei project to both the cochlear nucleus and the inferior colliculus by way of axon collaterals: a fluorescent retrograde double-labeling study in the rat. Neurosci Res 29:135–142.

Lorente de Nó R. 1981. The primary acoustic nuclei. New York: Raven Press.

Macron JM, Marlot D, Duron B. 1985. Phrenic afferent input to the lateral medullary reticular formation of the cat. Respir Physiol 59:155–167.

Maki K, Furukawa S. 2005. Acoustical cues for sound localization by the Mongolian gerbil, *Meriones unguiculatus*. J Acoust Soc Am 118:872–86.

Manis PB. 1989. Responses to parallel fiber stimulation in the guinea pig dorsal cochlear nucleus in vitro. J Neurophysiol 61:149–161.

Matsushita M, Ikeda M. 1976. Projections from the lateral reticular nucleus to the cerebellar cortex and nuclei in the cat. Exp Brain Res 24:403–421.

McDonald DM, Rasmussen GL. 1971. Ultrastructural characteristics of synaptic endings in the cochlear nucleus having acetylcholinesterase activity. Brain Res 28:1–18.

Menetrey D, Roudier F, Besson JM. 1983. Spinal neurons reaching the lateral reticular nucleus as studied in the rat by retrograde transport of horseradish peroxidase. J Comp Neurol 220:439–452.

Mizuno N, Nakamura Y. 1973. An electron microscopic study of spinal afferents to the lateral reticular nucleus of the medulla oblongata in the cat. Brain Res 53:187–191.

Mugnaini E, Morgan JI. 1987. The neuropeptide cerebellin is a marker for two similar neuronal circuits in rat brain. Proc Natl Acad Sci U S A 84:8692–8696.

Mugnaini E, Osen KK, Dahl AL, Friedrich VL Jr, Korte G. 1980a. Fine structure of granule cells and related interneurons (termed Golgi cells) in the cochlear nuclear complex of cat, rat and mouse. J Neurocytol 9:537–570.

Mugnaini E, Warr WB, Osen KK. 1980b. Distribution and light microscopic features of granule cells in the cochlear nuclei of cat, rat, and mouse. J Comp Neurol 191:581–606.

Musicant AD, Chan JC, Hind JE. 1990. Direction-dependent spectral properties of cat external ear: new data and cross species comparisons. J Acoust Soc Am 87:757–781.

Newlands SD, Perachio AA. 2003. Central projections of the vestibular nerve: a review and single fiber study in the Mongolian gerbil. Brain Res Bull 60:475–495.

Oertel D, Young ED. 2004. What's a cerebellar circuit doing in the auditory system? Trends Neurosci 27:104–110.

Ohlrogge M, Doucet JR, Ryugo DK. 2001. Projections of the pontine nuclei to the cochlear nucleus in rats. J Comp Neurol 436:290–303.

Parenti R, Cicirata F, Panto MR, Serapide MF. 1996. The projections of the lateral reticular nucleus to the deep cerebellar nuclei. An experimental analysis in the rat. Eur J Neurosci 8:2157–2167.

Paxinos G, Watson C. 1998. The rat brain in stereotaxic coordinates. New York: Academic Press.

Qvist H, Dietrichs E. 1985. The projection from the superior colliculus to the lateral reticular nucleus in the cat as studied with retrograde transport of WGA-HRP. Anat Embryol 173:269–274.

Qvist H, Dietrichs E. 1986. Afferents to the lateral reticular nucleus from the oculomotor region. I. The Edinger-Westphal nucleus. Anat Embryol 175:261–269.

Rajakumar N, Hrycyshyn AW, Flumerfelt BA. 1992. Afferent organization of the lateral reticular nucleus in the rat: an anterograde tracing study. Anat Embryol 185:25–37.

Rao KR, Ben-Arie J. 1996. Optimal head related transfer functions for hearing and monaural localization in elevation: a signal processing design perspective. IEEE Trans Biomed Eng. 43:1093–105.

Rice JJ, May BJ, Spirou GA, Young ED. 1992. Pinna-based spectral cues for sound localization in cat. Hear Res 58:132–152.

Ruigrok TJ, Cella F, Voogd J. 1995. Connections of the lateral reticular nucleus to the lateral vestibular nucleus in the rat. An anterograde tracing study with *Phaseolus vulgaris* leucoagglutinin. Eur J Neurosci 7:1410–1413.

Ryugo DK, Haenggeli CA, Doucet JR. 2003. Multimodal inputs to the granule cell domain of the cochlear nucleus. Exp Brain Res 153:477–485.

Shintani T, Mori RL, Yates BJ. 2003. Locations of neurons with respiratory-related activity in the ferret brainstem. Brain Res 974: 236–242.

Shokunbi MT, Hrycyshyn AW, Flumerfelt BA. 1985. Spinal projections to the lateral reticular nucleus in the rat: a retrograde labelling study using horseradish peroxidase. J Comp Neurol 239:216–226.

Shore SE. 2005. Multisensory integration in the dorsal cochlear nucleus: unit responses to acoustic and trigeminal ganglion stimulation. Eur J Neurosci 21:3334–3348.

Shore SE, Vass Z, Wys NL, Altschuler RA. 2000. Trigeminal ganglion innervates the auditory brainstem. J Comp Neurol 419:271–285.

Stocker SD, Steinbacher BC Jr, Balaban CD, Yates BJ. 1997. Connections of the caudal ventrolateral medullary reticular formation in the cat brainstem. Exp Brain Res 116:270–282.

Walberg F, Dietrichs E, Nordby T. 1985. On the projections from the vestibular and perihypoglossal nuclei to the spinal trigeminal and lateral reticular nuclei in the cat. Brain Res 333:123–130.

Weedman DL, Ryugo DK. 1996. Projections from auditory cortex to the cochlear nucleus in rats: synapses on granule cell dendrites. J Comp Neurol 371:311–324.

Weedman DL, Pongstaporn T, Ryugo DK. 1996. An ultrastructural study of the granule cell domain of the cochlear nucleus in rats: mossy fiber endings and their targets. J Comp Neurol 369:345–360.

Weinberg RJ, Rustioni A. 1987. A cuneocochlear pathway in the rat. Neuroscience 20:209–219.

Wolff A, Künzle H. 1997. Cortical and medullary somatosensory projections to the cochlear nuclear complex in the hedgehog tenrec. Neurosci Lett 221:125–128.

Wright DD, Ryugo DK. 1996. Mossy fiber projections from the cuneate nucleus to the cochlear nucleus in the rat. J Comp Neurol 365:159–172.

Wu HS, Sugihara I, Shinoda Y. 1999. Projection patterns of single mossy fibers originating from the lateral reticular nucleus in the rat cerebellar cortex and nuclei. J Comp Neurol 411:97–118.

Yates BJ, Stocker SD. 1998. Integration of somatic and visceral inputs by the brainstem: functional considerations. Exp Brain Res 119:269–275.

Ye Y, Kim DO. 2001. Connections between the dorsal raphe nucleus and a hindbrain region consisting of the cochlear nucleus and neighboring structures. Acta Otolaryngol 121:284–288.

Zhan X, Pongstaporn T, Ryugo DK. 2006. Projections of the second cervical dorsal root ganglion to the cochlear nucleus in rats. J Comp Neurol 496:335–348.

Zhou J, Shore S. 2004. Projections from the trigeminal nuclear complex to the cochlear nuclei: a retrograde and anterograde tracing study in the guinea pig. J Neurosci Res 78:901–907.